Amorphous silicon-liquid crystals device for photonic applications

A. Fuentes-Garcia, M. C. Grados-Luyando, J. C. Ramirez-San-Juan, and R. Ramos-Garcia*

National Institute of Astrophysics, Optics and Electronics, Optics Department, Apartado Postal 51 y 216, Puebla Pue, 72000 Mexico
**rgarcia@inaoep.mx*

Abstract: We demonstrate that an hydrogenated amorphous silicon (a:Si-H)-liquid crystals hybrid device could be used for the recording of high resolution (0.8-2 μm) dynamic holograms. A maximum diffraction efficiency of 3.3% was obtained at low power (1.5 mW) He-Ne laser. The nonlinear refractive index change at 0.6 W/cm^2 is $n_2 \sim 1x10^{-2}$ cm^2/W, although small compared to that obtained in dye-doped liquid crystal, is equal to the reported in pure liquid crystal although with much higher power density (~50 W/cm^2). The device operates in the red to near-infrared part of the spectrum which makes it attractive due to its potential applications in telecommunications and military applications.

OCIS codes: (190.0190) Nonlinear optics; (050.1950) Diffraction gratings; (090.0090) Holography; (160.3710) Liquid crystals.

References and links

1. P. Y. Chiou, A. T. Ohta, and M. C. Wu, "Massively parallel manipulation of single cells and microparticles using optical images," Nature **436**(7049), 370–372 (2005).
2. P. Y. Chiou, "Massively parallel optical manipulation of single cells, micro- and nano-particles on optoelectronic devices," PhD Dissertation (University of California at Berkeley, 2005).
3. A. Brignon, I. Bongrand, B. Loiseaux, and J. P. Huignard, "Signal-beam amplification by two-wave mixing in a liquid-crystal light valve," Opt. Lett. **22**(24), 1855–1857 (1997).
4. N. V. Tabiryan and C. Umeton, "Surface-activated photorefractivity and electro-optic phenomena in liquid crystals," J. Opt. Soc. Am. B **15**(7), 1912–1917 (1998).
5. D. R. Evans and G. Cook, "Bragg-matched photorefractive two-beam coupling in organic-inorganic hybrids," J. Nonlinear Opt. Phys. Mater. **16**(03), 271–280 (2007).
6. R. Ramos-Garcia and C. Berrospe-Rodriguez, "Enhancement of the coupling gain in GaAs-liquid crystal hybrid devices," Mol. Cryst. Liq. Cryst. (Phila. Pa.) **561**(1), 68–73 (2012).
7. R. A. Street, *Hydrogenated Amorphous Silicon* (Cambridge University Press, 1991).
8. J. H. Wei and S. C. Lee, "Electrical and optical properties of implanted amorphous silicon," J. Appl. Phys. **76**(2), 1033–1040 (1994).
9. R. Schwarz, F. Wang, and M. Reissner, "Fermi-level dependence of the ambipolar diffusion length in amorphous-silicon thin-film transistors," Appl. Phys. Lett. **63**(8), 1083–1085 (1993).
10. H. A. Pohl, *Dielectrophoresis: The Behavior of Neutral Matter in Nonuniform Electric Fields* (Cambridge University Press, 1978).
11. I. C. Khoo, *Liquid Crystals* (Wiley, 1995).
12. V. G. Bondar, O. D. Lavrentovich, and V. M. Pergamenshchik, "Threshold of structural hedgehog-ring transition in drops of a nematic in an alternating electric field," Pis'ma Zh. Eksp. Teor. Fiz. **101**, 111–125 (1995).
13. W. Beyer and B. Hoheisel, "Photoconductivity and dark conductivity of hydrogenated amorphous silicon," Solid State Commun. **47**(7), 573–576 (1983).
14. A. T. Ohta, P.-Y. Chiou, H. L. Phan, S. W. Sherwood, J. M. Yang, A. N. K. Lau, H.-Y. Hsu, A. Jamshidi, and M. C. Wu, "Optically controlled cell discrimination and trapping using optoelectronic tweezers," IEEE J. Sel. Top. Quantum Electron. **13**(2), 235–243 (2007).
15. S. L. Neale, M. Mazilu, J. I. B. Wilson, K. Dholakia, and T. F. Krauss, "The resolution of optical traps created by light induced dielectrophoresis (LIDEP)," Opt. Express **15**(20), 12619–12626 (2007).
16. M. Herrington, K. Daly, O. Buchnev, G. D'Alessandro, and M. Kaczmarek, "AC-field–enhanced beam coupling in photorefractive hybrid liquid crystals," EPL **95**(1), 14003–14009 (2011).

#185053 - $15.00 USD Received 7 Feb 2013; revised 5 Apr 2013; accepted 8 Apr 2013; published 1 May 2013

17. H. G. Kreul, S. Urban, and A. Würflinger, "Dielectric studies of liquid crystals under high pressure: Static permittivity and dielectric relaxation in the nematic phase of pentylcyanobiphenyl (5CB)," Phys. Rev. A **45**(12), 8624–8631 (1992).
18. M. Gu, Y. Yin, S. V. Shiyanovskii, and O. D. Lavrentovich, "Effects of dielectric relaxation on the director dynamics of uniaxial nematic liquid crystals," Phys. Rev. E Stat. Nonlin. Soft Matter Phys. **76**(6), 061702 (2007).
19. F. Simoni, O. Francescangeli, Y. Reznikov, and S. Slussarenko, "Dye-doped liquid crystals as high-resolution recording media," Opt. Lett. **22**(8), 549–551 (1997).
20. I. C. Khoo, P. H. Chen, M. Y. Shih, A. Shishido, S. Slussarenko, and M. V. Wood, "Supra optical nonlinearities (SON) of methyl red- and azobenzene liquid crystal-doped nematic liquid crystals," Mol. Cryst. Liq. Cryst. (Phila. Pa.) **358**(1), 1–13 (2001).
21. B. Ya. Zel'dovich, N. F. Pilipetskii, A. V. Sukhov, and N. V. Tabiryan, "Giant optical nonlinearity in the mesophase of a nematic liquid crystal (NLC)," Pis'ma Zh. Eksp. Teor. Fiz. **31**, 287–292 (1980).
22. R. Porras Aguilar, J. C. Ramirez-San-Juan, O. Baldovino-Pantaleon, D. May-Arrioja, M. L. Arroyo Carrasco, M. D. Iturbe-Castillo, D. Sánchez-de-la-Llave, and R. Ramos-Garcia, "Polarization-controlled contrasted images using dye-doped nematic liquid crystals," Opt. Express **17**(5), 3417–3423 (2009).

1. Introduction

Optodielectrophoresis (ODEP) is a novel dielectrophoretic technique were virtual electrodes are created by illumination of photoconducting electrodes, dispensing the need of fabricating real electrodes. ODEP was proposed in 2005 by the group of Prof. Wu at Berkeley University as a technique intended for massive manipulation of microparticles [1]. It was shown that up to 15000 particles could be manipulated simultaneous with a diode light source of only a couple of mW power [1]. The device consists of thin layer of water containing the microparticles sandwiched between a photoconductive hydrogenated amorphous silicon (a:Si-H) substrate and an ITO covered glass-plate [1,2]. An AC electric field is applied between the electrodes. Under dark conditions, the resistivity of the a:Si-H is much larger than the water's resistivity, so the voltage drops mainly on the a:Si-H, however, under illumination the situation reverse and the voltage drops on the water layer. Thus, a spatially modulated electric field inside the water is controlled by illumination allowing manipulation of microparticles [1,2].

Hybrid devices based on liquid crystals and inorganic photoconductors are subject of intensive research since they combine the large optical anisotropy of liquid crystals and photoinduced space-charge fields in photoconductors to enhance the energy exchange in beam coupling experiments [3–6]. Photorefractive crystals have been the choice of photoconductor material in these devices [4–6] because high space-charge fields can be achieved with relative low power lasers, which combined with the large refractive index anisotropy of liquid crystals, produce extremely large beam coupling gain coefficients [5,6]. However, the cost of photorefractive crystals and their lack of reproducibility on its properties have hindered its widespread use. On the contrary, a:Si-H is a widely used material in the solar cell and display industries with well known electrical and optical properties [7,8]. In addition, the high density of defect states of a:Si-H results in highly absorbent material which combined with its short ambipolar diffusion length [9] ~100nm, results in a good photoconductive material for patterning high resolution virtual electrodes. In this work, we show that the electric field obtained by ODEP can be effectively used to reorient liquid crystals and thus, produce dynamic holograms with all the advantages of ODEP.

2. Optodielectrophoresis

The dielectrophoretic force (DEP) on a dielectric particle immersed in an inhomogeneous electric field is giving by [10]:

$$\left\langle \boldsymbol{F}_{DEP}(t)\right\rangle = 2\pi r^3 \varepsilon_m \,\mathrm{Re}[K^*(\omega)]\nabla\left|\boldsymbol{E}(t)\right|^2, \tag{1}$$

$$\mathrm{K}^*(\omega) = \frac{\varepsilon_p^* - \varepsilon_m^*}{\varepsilon_p^* + 2\varepsilon_m^*}, \quad \varepsilon_p^* = \varepsilon_p - i\frac{\sigma_p}{\omega}, \quad \varepsilon_m^* = \varepsilon_m - i\frac{\sigma_m}{\omega}, \tag{2}$$

#185053 - $15.00 USD Received 7 Feb 2013; revised 5 Apr 2013; accepted 8 Apr 2013; published 1 May 2013

where $<\boldsymbol{F}_{DEP}(t)>$ represents a temporal average of the dielectrophoretic force $\boldsymbol{F}(t)$ and $\boldsymbol{E}(t)$ is the electric field on a particle of radius r. $\varepsilon_{p,m}$, and $\sigma_{p.m}$ are the dielectric permittivity and conductivity of the particle and the media, respectively, ω is the frequency of applied field and $K^*(\omega)$ is the Clausius-Mossotti factor. Note that the DEP depend on the spatial gradients of the square modulus of the electric field. Contrary to optical tweezers, the same particle may be attracted or repelled from the highest gradient electric field as the Clausius-Mossotti factor switch sign with the frequency [10]. The AC electric field is applied between custom-designed electrodes, usually fabricated with photolithographic techniques, which are cumbersome and expensive to fabricate. On the contrary, in ODEP the spatial light distribution creates dynamic virtual electrodes in almost real time [1,2], dispensing the need of fabrication of electrodes.

In this work, we replace the colloidal solution used in ODEP experiments with undoped 5CB nematic liquid crystal. By doing so, we intend to use the electric field distribution produced inside the hybrid device to reorient the liquid crystal molecules. The determination of the forces exerted on the liquid crystal molecules is not important for our purposes, and only the torque exerted by the electric field inside the liquid crystal will be relevant. The electric torque Γ_E exerted on the liquid crystals is given by [11] $\Gamma_E = \Delta\varepsilon(n\cdot E)(n\times E)$, where $\Delta\varepsilon$ is the dielectric anisotropy of the liquid crystal, $\boldsymbol{n}$ is the director axis and the evanescent electric field $\boldsymbol{E}$ is obtained numerically, as described below. As shown in [2], the spatial distribution of the electric field inside the liquid is not a simple one. In general, numerical methods are employed to find it. In absence of illumination, the electric field inside the LC is constant (except, of course, near the device's boundaries). If spatially periodic illumination, produced by the interference of pair of coherent beams from a laser, impinges on the device, then spatially periodic reconfigurable electrodes will be created by light. The spatially varying electric field is expected to modulate the refractive index of the liquid crystal creating thus, a hologram. The electric field inside the liquid crystals and a:Si are both dependent on the frequency of the externally applied field and, hence, the torque exerted on the liquid crystals molecules will also be frequency-dependent.

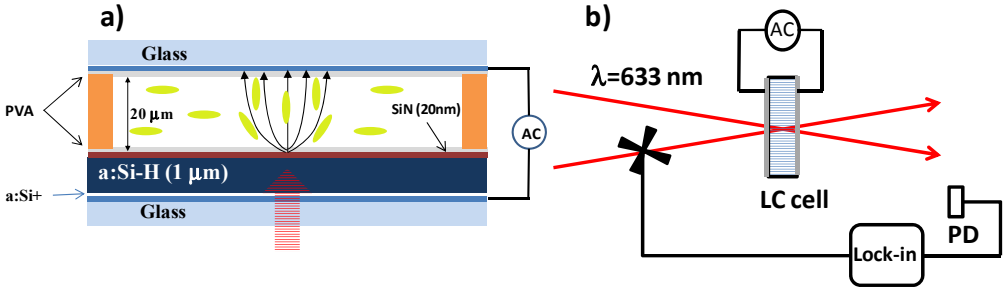

Fig. 1. a) The red arrow represents the laser beam entering by the side of the photoconductor film. The photogenerated electric field reorients the liquid crystals molecules on the illuminated area, outside of which, the electric field is negligible. The liquid crystal molecules are aligned parallel to the substrate before illumination. b) Experimental set up for hologram recording in a:Si-liquid crystal hybrid device. Thick lines represent the transmitted beams (zero-order beams) while the weaker ones represent the first diffracted order beams.

3. Experiment description

A schematic diagram of the device used in this work is shown in Fig. 1a. It consists of couple of glass plates with indium thin oxide (ITO) electrodes deposited on them. On top of one of the ITO electrodes, a polyvinyl alcohol (PVA) aligning rubbing film was deposited by spin-coating and rubbed unidirectionally with a soft tissue. On the other glass plate, a thin film of 50 nm of highly doped amorphous silicon (a:Si^+) was deposited on top of the ITO electrode in order to reduce the resistance contact. Then, 1 µm thick film of a:Si-H, grown at 230°C, was

#185053 - $15.00 USD Received 7 Feb 2013; revised 5 Apr 2013; accepted 8 Apr 2013; published 1 May 2013

deposited on top of a:Si^+ followed by a 20 nm dielectric thin film of a silicon nitride (SiN). Finally, a PVA aligning layer was deposited and rubbed on the same direction as the previous one. The SiN dielectric film has two purposes: avoid electrical contact between the LC and the a:Si-H and protection of the a:Si-H film. 20 μm microparticles spacers were placed between the glass plates. Two extremes of the cell were glued with an epoxy resin. Finally, the 5CB liquid crystal was heat up above its nematic-isotropic phase transition temperature (35°C) and the cell was filled in by capillarity and sealed it.

Two coherent beams from a He-Ne laser (λ = 633nm) interfere on the sample to produce a sinusoidal light distribution, as shown in Fig. 1b. This intensity distribution will determine the photoinduced electrode configuration. The beams of equal power (0.75 mW) are obtained using an unpolarized beam splitter. The intersection angle between the beams can be adjusted to change the grating period of the interference pattern. Using a function generator, a sinusoidal AC field is applied to the cell whilst illuminated. One of the beam is chopped at a frequency of ~1 kHz, which is much larger than the inverse of the response time (~tens of milliseconds), in order to reduce the noise on the diffracted signal. Detection is carried out with a fast photodetector connected to a lock-in amplifier, and this in its turn, is controlled by a computer. The sample can be considered as thin (20 μm) since several diffracted orders are produced. In fact, for the grating periods used in the experiment d/Λ~10-25, which lies in the limit of the Raman-Nath regime. The reported diffraction efficiency will always be measured on the first-order of diffraction (Eq. (3)). This was determined by measuring the transmitted beam intensity I_0 of one of the beams and its corresponding first order beam I_1 intensity with the voltage applied. The largest diffraction efficiency measured is small ~3.3%, so the diffraction efficiency of the first order can be approximated by the argument of the first-order Bessel function, i.e. $J_1(x)\sim x/2$,

$$\eta_1 = \frac{I_1}{I_1 + I_0} = J_1^2(2\pi n_2 Id/\lambda) \approx (\pi n_2 Id/\lambda)^2, \quad (3)$$

where n_2 is the nonlinear refractive index, d is the liquid crystal thickness, I the total beam intensity and λ is the wavelength of the laser beam. From Eq. (3), the nonlinear refractive index can be easily calculated. It is worth to mention that no hologram recording could be achieved if the applied field is off. This indicated that the laser beam itself is unable to reorient the LC molecules.

4. Results and discussion

In order to obtain the electric field distribution within the LC cell, the quasi-static approximation of the AC/DC module of Comsol Multiphysics was used. In the model (see Fig. 2), only the liquid crystal (20 μm) and a:Si film (1 μm) play a role in determining the electric field [1,2]. In the simulation, a conductivity of $3\text{x}10^{-6}$ S/m [12] and 10^{-8} S/m (in the dark [13]) were assumed for LC and a:Si-H, respectively. It was also assumed that the electrical conductivity is uniform inside the a:Si-H film and the photoconductivity is a linear function of the illumination intensity [14]. In order to understand the behavior of the electric field inside the liquid crystal, a single Gaussian beam (17 μm beam radius) is incident from below and propagates along the + z direction. For the simulation, an applied voltage of 10 V is assumed. The *x-axis* is parallel to liquid crystal-a:Si-H interface. Given the axial symmetry of the problem, Comsol Multiphysics reduce the problem to only half of the cell as shown in Fig. 2.

#185053 - $15.00 USD Received 7 Feb 2013; revised 5 Apr 2013; accepted 8 Apr 2013; published 1 May 2013

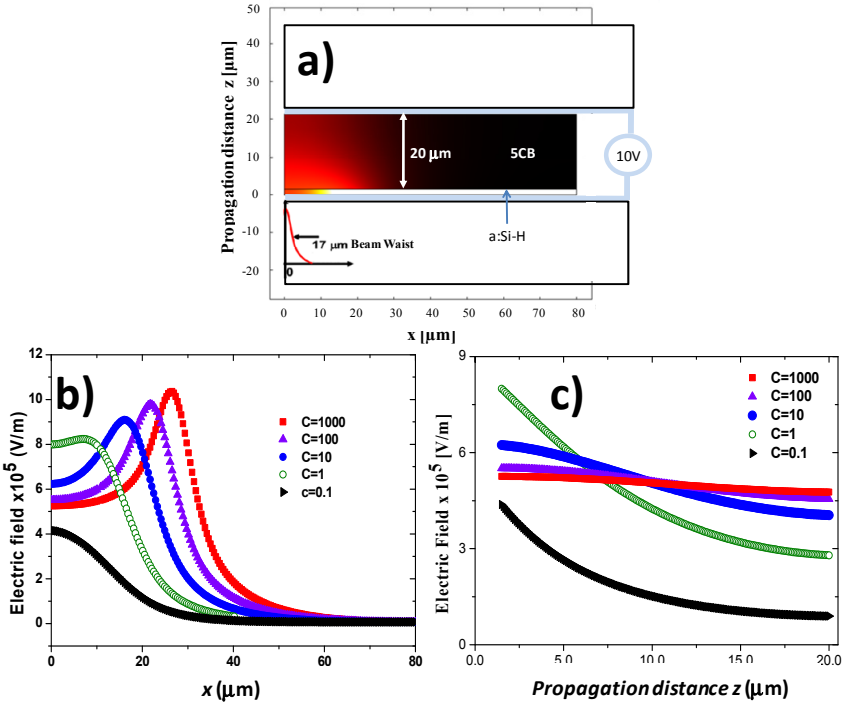

Fig. 2. a) Geometry of the model and distribution of the electric field (red zone) inside the liquid crystal. b) Electric field profiles along the lateral distance measure 1 µm above the amorphous silicon when an applied field of 10 V and a Gaussian beam waist of 17 µm were used. c) Electric field distribution along the propagation distance. The variable C is defined as σ_{aSi}/σ_{LC}, where σ_{aSi} represents the a:Si photoconductivity at the peak of the Gaussian beam and σ_{LC} the conductivity of the liquid crystal. The peak photoconductivity equals the liquid crystal conductivity when $C = 1$.

In our simulations, the peak photoconductivity of the amorphous silicon (σ_{aSi}) is normalized to the conductivity of the liquid crystal (σ_{LC}), i.e $C = \sigma_{aSi}/\sigma_{LC}$. For $C<<1$ the electric field drops mainly on the amorphous silicon while for $C>>1$ does it on the liquid crystal. Note that at regions where there is no light, the resistance of a:Si is higher than that of LC, so most of the field drops in a:Si. Under illumination, the situation reverses, as indicated in Fig. 2a. Figure 2b shows the electric field profiles inside the liquid crystal along the lateral distance measured 1 µm above the amorphous silicon. Note that the electric field far from the illuminated region is practically zero and, therefore, no reorientation is expected. For $C = 0.1$, only 40% of the field drops inside the liquid crystal and therefore liquid crystal reorientation may be achieved. For $C = 1$, the virtual electrodes has been fully turned on, and larger values of C only increases the spatial extension of the virtual electrode, reducing the spatial resolution of the device [15]. In addition, the electric field inside the liquid crystal becomes double peaked. Thus, higher intensity not necessarily means higher electric field or enhanced reorientation of liquid crystals. In Fig. 2c it is shown that the electric field along the propagation distance. For C>1 it is practically constant, while for C<<1 the electric field is weaker and shows an evanescent behavior. On the other hand, the electric field seem largest when C = 1.

#185053 - $15.00 USD Received 7 Feb 2013; revised 5 Apr 2013; accepted 8 Apr 2013; published 1 May 2013

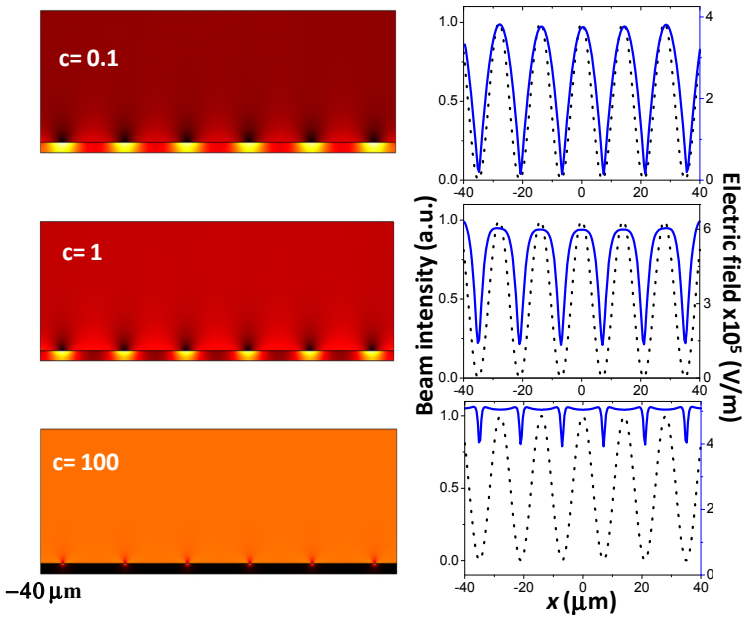

Fig. 3. Electric field profiles produced by sinusoidal illumination. Left column shows the electric field spatial distribution inside the liquid crystal for several power values, equivalently C values. The left column is a profile of the electric field obtained 1 mm above the amorphous silicon layer. For comparison, the intensity spatial distribution is also shown. Notice that the electric field is quite similar to the electric field for C<1 but practically becomes constant for C>>1.

When using sinusoidal illumination, as it was done in our experiment, the electric field inside the liquid crystal is expected to be a copy of the illumination pattern and therefore, a sinusoidal phase grating should be recorded. However, as anticipated before, this is true for $C \leq 1$. Figure 3, shows the spatial distribution of the electric field when periodic illumination, $I = I_0(1 + \cos kx)$, is employed for different C values. The right column shows the profile of the electric field (continuous line) measured 1 µm above the amorphous silicon. For comparison, the periodic illumination (dotted line) is also shown. Note that for $C = 0.1$, the electric field is almost a copy of the illumination pattern. For $C = 1$, higher harmonics begin to show up and its modulation depth decreases. For $C = 100$, the contrast almost disappear and the electric field is almost constant except over the illuminated region where high gradients of the field are achieved. Higher harmonics are expected to contribute to the phase grating. Thus, high laser intensity is detrimental for the spatial resolution of the device [15]. Although the simulations where performed using a quasi-static approximation they describe reasonable well the results in optodielectrophoresis experiments [1,2,15] and qualitatively well our results.

Diffraction from the non-sinusoidal phase grating and, in combination with small Q number (grating recording is on the Raman-Nath regimen), may result on the generation of several diffraction orders. So in order to avoid further complications, all our experiments were performed at very low power (1.5 mW). In Fig. 4a the diffraction efficiency was measured as a function of the modulation voltage at a fix modulation frequency of 500 KHz. There is a threshold voltage ~2 V, above which liquid crystal reorientation occurs, then it grows linearly up to a maximum of 3.3%. At ~8V reaches a plateau value and then decreases for higher voltage. At about 15 V, the diffraction efficiency is almost zero. This behavior can be easily understood as follow: as the voltage increases, it does the reorientation of the liquid crystals until it reaches its full reorientation. For voltages larger than 10V, reorientation on the non-illuminated regions also takes place, reducing the contrast of the phase grating and thus, the diffraction efficiency.

#185053 - $15.00 USD Received 7 Feb 2013; revised 5 Apr 2013; accepted 8 Apr 2013; published 1 May 2013

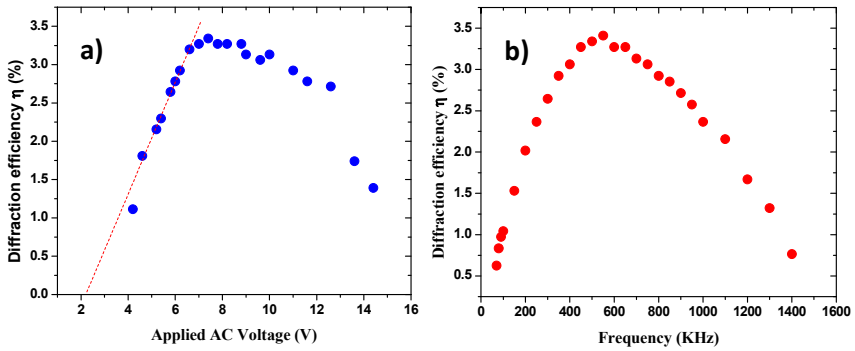

Fig. 4. a) The diffraction efficiency was measured as a function of the modulation voltage at a modulation frequency of 500 KHz. b) Diffraction efficiency vs modulation frequency at 8V.

The diffraction efficiency versus frequency shown in Fig. 4b follows a similar behavior as that of Fig. 4a. It growths at low frequency, saturates at ~600 KHz and then decrease almost linearly for higher frequency. This feature of the device is accounted for the frequency dependent impedance of the device, which consist of several thin films as described above. In fact, it has been shown that the different layers of the device can be modeled as serially connected lumped circuit elements [2,16]. The corresponding impedance of the n-film is given by

$$Z_n = \frac{R_n}{1 + i\omega R_n C_n}, \tag{4}$$

where $R_n = L_n/(\sigma_n A)$ is the resistance and $C_n = \varepsilon_0 \varepsilon_n A/L_n$, is the capacitance. Here, L is the thickness of the film, A the area of the device, σ the conductance, ε the relative permitiviy, ε_0 the permitivity of free space and ω the modulation frequency. In the original device employed for ODEP, it was shown that the only relevant films for the device operation are the water and amorphous silicon impedance. Our device is almost identical to the one reported in [1], except that water was replaced by liquid crystal and two aligning layers were added. The impedance of the aligning layers is dominated by capacity effects as well as that of SiN film and the electric double layer, with values much smaller than the impedance of the a:Si or liquid crystal [2]. For such reason, in our analysis only the liquid crystal and amorphous silicon impedances will be studied.

Figure 5 shows the impedance of the liquid crystal and amorphous silicon as function of the modulation frequency. For ω<30kHz, most of the field drops on the amorphous silicon and therefore no reorientation of the liquid crystal occurs. For ω>30kHz, the liquid crystal impedance dominates and the device is activated. The inset shows the difference between impedances of the liquid crystal (Z_{lc}) and a:Si (Z_{aSi}). The theory predicts that a plateau should be reached for ω>0.5 MHz. In this case, the impedance of the liquid crystal and the a:Si are given by $Z_x = iR_x\sigma_x/(\omega\varepsilon_0\varepsilon_x) = iL_x/(\omega\varepsilon_0\varepsilon_x)$, where $x = lc, aSi$. For these conditions, the difference in impedance is constant, explaining the inset of Fig. 5. However, the experiment shows that the diffraction efficiency decays in the 0.6-1.4 MHz range. Although, the dielectric permittivity of the liquid crystals is frequency-dependent, for the ω = 0.1-1 MHz range, the dielectric permittivity behavior is constant [17,18]. So, we do not have an explanation for this behaviour and more detailed studies are necessary.

Note that one can reduce the activation frequency of the device (see Fig. 5) by moving the crossing point between the LC and a:Si-H impedance. This can be achieved by reducing the capacitance impedance of a:Si-H, i.e. by decreasing its thickness or by increasing the resistivity of LC.

#185053 - $15.00 USD Received 7 Feb 2013; revised 5 Apr 2013; accepted 8 Apr 2013; published 1 May 2013

Finally, the resolution of the device was measured by changing the angle between the writing beams. From Fig. 6, at 0.8 µm a diffraction efficiency of *0.5%* was obtained and it quickly saturates for periods >2 µm. These results compare quite well with results presented by Simoni et al [19]. This is not surprising considering that the spatial resolution is determined by the liquid crystal itself and not the amorphous silicon. Remember that the ambipolar diffusion length [9] is *~0.1 µm* and therefore is possible to record even higher resolution holograms. Using Eq. (3), the maximum nonlinear refractive index change is $\sim 1x10^{-2}\ cm^2/W$, which is small compared to that obtained in dye-doped liquid crystal [20], but equal to the reported by Zeldovich et al [21] by focusing a 10 mW He-Ne laser (~50 W/cm^2) in pure liquid crystal.

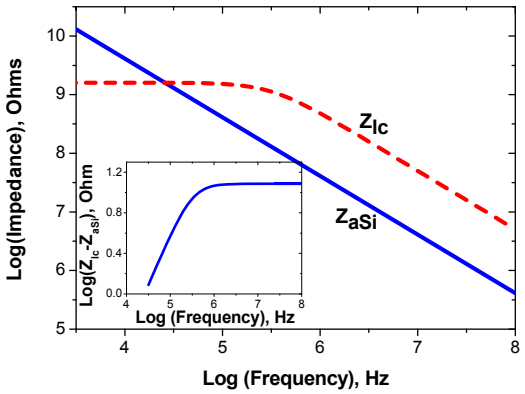

Fig. 5. Impedance of the liquid crystal film (Z_{lc}) and the amorphous silicon (Z_{aSi}) as function of modulation frequency. For ω<30kHz, most of the field drops on the amorphous silicon and no reorientation of the liquid crystal occurs. For ω>30kHz, the liquid crystal impedance dominates and the device is activated. In the inset, the difference between impedances is shown.

In our experiments, an unfocused 1.5 mW He-Ne laser (0.6 W/cm^2) was used, i.e. a power density almost two orders of magnitude smaller. Although the device works fine, there is plenty of room for optimization. For example by changing the temperature up to 33% diffraction efficiency has been achieved, however, the phenomenon is not reproducible and more detailed experiments are needed. This device could be applied for phase contrast applications in the visible to near-infrared part of the spectrum because tunable, real-time phase filter could easily be recorded [22].

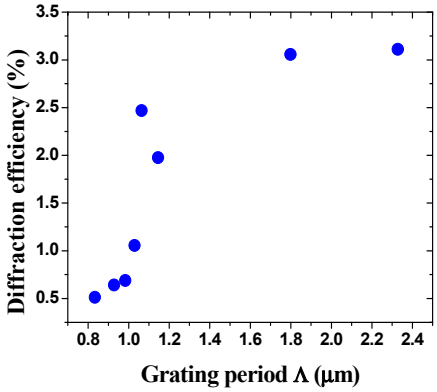

Fig. 6. The maximum diffraction efficiency of ~3.3% is achieved around 8V and a frequency of 500 kHz.

#185053 - $15.00 USD Received 7 Feb 2013; revised 5 Apr 2013; accepted 8 Apr 2013; published 1 May 2013

5. Conclusions

We propose a novel hybrid device for dynamic hologram recording based on hydrogenated amorphous silicon (a:Si-H) and 5Cb liquid crystals. Here, no electrode fabrication is needed since they are created by the light distribution incident onto a photoconducting material. High spatial resolution (0.8-2 μm) holograms with maximum diffraction efficiency of 3.3% were obtained at low power (1.5 mW) He-Ne laser. In addition, a nonlinear refractive index $n_2 \sim 1x10^{-2}\ cm^2/W$ was obtained. This value although small, is one of the largest reported so far in pure liquid crystal using unfocused He-Ne lasers. Near-infrared operation is attractive due to its potential applications in telecommunications and military applications.

Acknowledgments

The authors appreciate sample preparation by Prof. Pere Roca I Cabarrocas from L'École Polytechnique, Cedex, France. We also appreciate financial support from CONACyT through project CB-2010-153463.

#185053 - $15.00 USD Received 7 Feb 2013; revised 5 Apr 2013; accepted 8 Apr 2013; published 1 May 2013